# Multi-scale analysis of a porous carbonate rock under triaxial conditions

Catherine Doré-Ossipyan, Jean Sulem, Michel Bornert, Alexandre Dimanov, Patrick Aimedieu, Vincent de Greef, Andrew King

# Multi-scale analysis of a porous carbonate rock under triaxial conditions

Catherine Doré-Ossipyan
*Laboratoire Navier, ENPC, Université Gustave Eiffel, CNRS UMR 8205, 77455 Marne-la-Vallée, France*
*Laboratoire de Mécanique des Solides, CNRS UMR 7649, École Polytechnique, 91128 Palaiseau, France*

Jean Sulem
*Laboratoire Navier, ENPC, Université Gustave Eiffel, CNRS UMR 8205, 77455 Marne-la-Vallée, France*

Michel Bornert
*Laboratoire Navier, ENPC, Université Gustave Eiffel, CNRS UMR 8205, 77455 Marne-la-Vallée, France*

Alexandre Dimanov
*Laboratoire de Mécanique des Solides, CNRS UMR 7649, École Polytechnique, 91128 Palaiseau, France*

Patrick Aimedieu
*Laboratoire Navier, ENPC, Université Gustave Eiffel, CNRS UMR 8205, 77455 Marne-la-Vallée, France*

Vincent de Greef
*Laboratoire de Mécanique des Solides, CNRS UMR 7649, École Polytechnique, 91128 Palaiseau, France*

Andrew King
*Psiche beamline, Synchrotron Soleil, 91192, Saint Aubin, France*

ABSTRACT: The formation and evolution of deformation bands in a carbonate rock with high porosity is investigated by performing in situ triaxial experiments with high-resolution synchrotron X-Ray Computed Tomography by placing a specifically designed testing device directly in the tomograph. The processing of images by Digital Volume Correlation techniques provides insight on the deformation modes of the samples for various loading conditions. In more porous specimens with a homogeneous microstructure, many subhorizontal compactant deformation bands sequentially initiate, propagate, widen and fully saturate the volume of the rock sample after a few percent of overall strain, leading to a rather uniform compaction of the sample. In contrast, denser samples with a more heterogeneous microstructure exhibit discrete deformation bands, in limited number. These bands propagate and widen, leading to strong localization of the deformation which remains restricted to certain parts of the sample.

*Keywords: in situ triaxial test, compaction bands, carbonate rocks, Digital Volume Correlation.*

## 1 INTRODUCTION

Porous sedimentary rocks have been of particular interest for a variety of application, such as gas exploitation, $CO_2$ sequestration and geothermal energy exploitation. Under high confinement, commonly met *in situ* during exploitation, experimental tests have shown (Baud et al. 2009, Huang et al. 2019, Leuthold et al. 2021) that strain in porous carbonate rocks is accommodated heterogeneously, with formation of thin tabular zones of localized compressive deformation, over a wide range of porosities. Similar observations stem from sandstones (Stanchits et al., 2009). These compaction bands (CBs) may develop as multiple discrete bands (Baud et al. 2017) or diffusively

(Papazoglou et al. 2017), appearing then as a band which widens with increasing effective stress. Due to the complex microstructure of carbonate rocks, caused by a large diversity of sedimentation processes and geologic history, identifying the micromechanisms that control inelastic compaction. Strain localization of carbonate rocks has been more challenging than in sandstones. In the presence of fluids, the development of compaction bands may significantly reduce permeability (Baud et al. 2009, Leuthold et al. 2021). It is therefore of paramount importance to understand the evolution of such a parameter with inelastic compaction.

Strain localization is a multiscale phenomenon, as it develops from the grain to the continuum scale. Micromechanisms responsible for the formation of deformation bands are associated with microstructural parameters, which also may vary from the grain to the continuum scale, leading to a variety of responses, even within the same rock (Baud et al. 2009)**.** These phenomena are studied on a dry carbonate rock, the Saint-Maximin limestone, which presents centimeter-scale microstructural heterogeneity, with alternating zones of higher and lower porosity zones. Its behavior was already characterized from standard size samples (4 cm in diameter), containing both types of zones (Abdallah 2020, Abdallah et al., 2021). A set of *in situ* triaxial experiments was performed on two sets of small samples (8 mm in diameter), cored within low-porosity (*dense*) and in high-porosity (*porous*) zones. Time-lapse high definition synchrotron 3D imaging (Psiché, beamline, Synchrotron Soleil, France) was used in order to understand the progressive strain localization from grain scale to continuum scale. The obtained 3D images are analyzed by Digital Volume Correlation (DVC), a full-field image processing method providing 3D displacement fields and strain maps (Lenoir et al, 2007). Among the twelve tests performed with various confining pressures on the two types on samples, we focus here on the results of triaxial tests performed at a confining pressure of 6 MPa. For standard size samples with a reference porosity of 38%, this confining pressure corresponds to the transition between brittle and ductile behavior (Abdallah et al. 2021).

## 2 MATERIAL AND METHOD

### *2.1 Material description and sample preparation*

The Saint-Maximin Limestone (SML) is a fine biocalcarenite, high porosity (38%) limestone from the Parisian basin, France, forming a grainstone, according to Dunham's classification. The blocks used are similar to those tested in a previous study by Abdallah et al. (2021). The location of dense and porous zones which alternate at a centimeter scale is random and no depositional structures are visible. Cylindrical samples of 8 mm in diameter and 16 mm in height were cored in both types of zones and scanned with our laboratory X-ray tomograph in order to select most homogeneous samples. For dense and porous samples, total porosity varies between 30 and 37%, and between 41 and 45%, respectively.

Small sub-angular dense calcite grains, foraminifera (miliolidae) shells with average diameters of 200 µm, are observed inside the porous zones (see Figure 1). Inter-granular porosity is abundant, as cementation is rare, and some pores are also found inside calcareous shells. Dense calcite grains appear larger (~300 µm) and more cemented inside dense zones, with an abundance of very large foraminifera (mean diameter ~500 µm). Most of the porosity of the dense zones is related to porosity occluded within the latter shells, but also to very large isolated inter-granular pores, and elongated pores with randomly distributed directions. Sub-rounded quartz grains are observed to be equally distributed in both zones, but their average diameter is slightly larger in dense ones (150 vs 100 µm).

### *2.2 Experimental set-up*

A recently developed *in situ* triaxial device allows to investigate mechanisms at the microstructural scale on representative samples. The triaxial testing device is composed of an uniaxial electromechanical actuator equipped with a force sensor, a confining pressure cell and pistons adapted to the different sample diameters (here 8 mm, with available setups for 4, 12 and 15 mm),

forming the main body of the testing device, an injection pump to inject water into the confining cell, and a pressure sensor.

The uniaxial rig is managed by controlling applied force or displacement rate. It is independent of the injection pump, but the axial force is servo-controlled together with confining pressure for application of hydrostatic loadings. The uniaxial loading capacity is of 10 kN, and a maximum confining pressure of 20 MPa can be achieved in the cell. The injection pump is a stainless steel syringe pump a 3 ml capacity. The pump injects water into the confining cell and is operated by controlling the flow rate manually. The device is placed inside the synchrotron optical hutch on the tomograph's rotation table (King et al, 2016). Samples are placed in between pistons inside the cell, isolated by a rubber jacket. A new helicoidal scanning procedure (8 rotations for a total height of 21.6 mm), has been developed to continuously scan the whole sample in about 12 minutes, despite the small height (3mm) of the X-Ray pink beam. It also allows to reduce ring artefacts and generates a single large volume instead of stacks of standard volumes. The chosen voxel size of 3.25 µm leads to volumes of over 100 Gb and ensures a detailed view of the micromechanisms acting at grain scale.

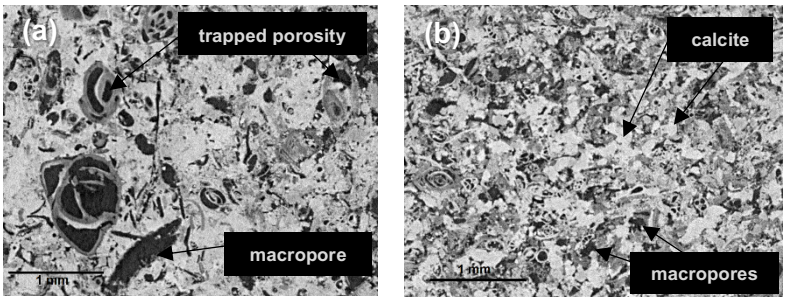


Figure 1. Cross sections through 3D XRCT images of intact dense (a) and porous (b) samples. Large calcite fossil shells (~500 µm) are observed in dense samples, containing microporosity. Intergranular porosity is more abundant in porous samples, with smaller calcite grains and shells (~150-200 µm).

Dense and porous samples were tested at confining pressures of 1, 3, 6, 8, 10.5 and 20 MPa. The axial load was applied with a displacement rate of 0.1 µm/s in the initial pre-yielding phase and 1 µm/s after yielding. Steps up to 200 µm (i.e. less than 1.25% incremental axial strain) between each scan were considered, in order to follow the progressive development of failure and avoid microstructural changes that would be too large for DVC analyses. Total axial shortening reached up to 50 %, except for samples tested at 3 and 8 MPa, which were less axially deformed in order to allow post mortem Scanning Electron Microscope observations. A total of 12 samples were tested.

Axial strain is estimated indirectly in real time from piston position corrected for setup compliance and is validated by post-processing 2D radiographs and the full 3D volumes by DVC.

## 3 RESULTS

First results from compression tests are presented. In Figure 2, the mean stress is plotted against the axial strain for the six samples of each type tested at different confining pressures. Small stress drops are due to relaxation of the sample during scans.; larger ones are associated with partial unloading.

For the porous samples (see Figure 2a), the hydrostatic part of the loading path (plotted in dotted black line) shows a critical value P* = 13 MPa for the onset of pore collapse. Further increase of effective stress is followed by strain hardening. Brittle behavior is observed for deviatoric loading under a confining pressure of 1 MPa. At a confining pressure of 3 MPa, the sample displayed a quasi-perfect plastic behavior, interpreted as the brittle/ductile transition. Triaxial tests at confining pressures above 6 MPa show an overall ductile behavior with linear hardening.

For the dense samples (see Figure 2b), no pore collapse was observed during hydrostatic test, up to 20 MPa which is the maximum capacity of the loading system. Brittle behavior is observed under a confining pressure of 1 MPa. For tests with a confining pressure between 3 and 10.5 MPa, a transitional regime is observed with no clear peak stress and a quasi-perfectly plastic response. The sample tested at 20 MPa shows a ductile behavior. The sample tested at 10.5 MPa exhibits a much

higher strength, probably due to its lower porosity (30%). Dense samples exhibit a significantly larger elastic domain than porous samples, despite the limited difference in porosity. This demonstrates the role of microstructural properties on the rock strength.

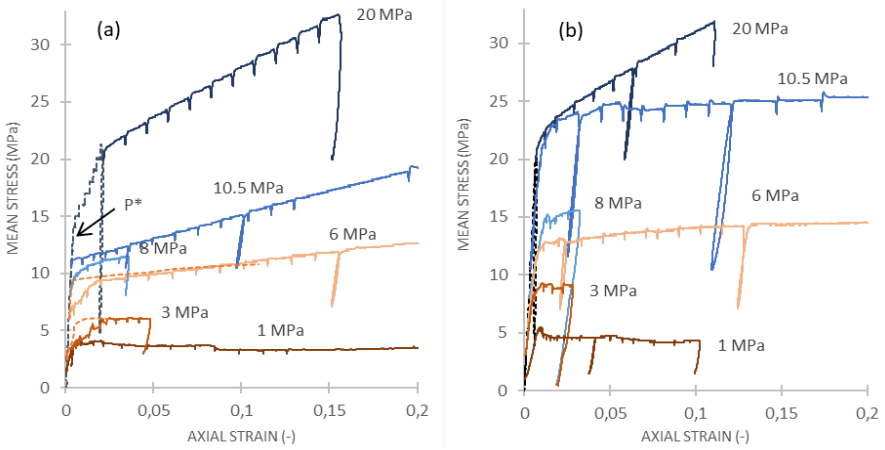


Figure 2. Triaxial compression tests with different confining pressures for (a) porous samples and (b) dense samples. Small stress drops correspond to pauses during tests for imaging.

### *3.1 Detailed analysis of the porous sample under a confining pressure of 6 MPa*

The porous sample at initial state presents a statistically rather homogeneous microstructure (see Figure 4a). Denser zones and more porous zones are visible at a millimeter-scale. The denser zones, with average porosities of about 35%, are due to local smaller intergranular pore space.

Cross-sections through total deformation maps, computed for a local gauge length of 100 voxels, i.e. 325 µm, at various stages of imposed axial strain are shown in Figure 4. Heterogeneous deformation in the form of multiple short subhorizontal compactant deformation bands randomly appear at the onset of yielding. They propagate towards the center of the sample with increasing axial strain until saturation of the sample. At an axial strain of 10%, the sample appears to be quasi homogeneously compacted, with a structuration of strain into many bands at small scale.

Reconstructed XRCT images reveal a global densification of the sample, starting at an axial strain of 1.3%. The average porosity is evaluated from mean grey level. It decreases linearly with the applied axial strain from 43% (before loading) to 34.7% at an axial strain of 12.5%. Compaction is mainly accommodated in weaker grains (crushing of dissolved calcite grains and shells). Computation of the local variation coefficient of grey levels (not shown here) reveals a homogenization of the porosity, as standard deviation of the grey level distribution decreases.

### *3.2 Detailed analysis of the dense sample under a confining pressure of 6 MPa*

For the dense sample, inspection of initial density map shows a slightly more porous zone in the lower part of the sample (see Figure 3a): porous inclusions are due to the presence of weak, smaller grains and less cementation. The typical size of local porosity fluctuations also appears larger than in the porous sample.

Deformation maps at various loading stages show (see Figure 3) that discrete compacting shear bands start to develop in the upper and lower parts of the sample, with two conjugate bands in the more porous zone. These two conjugate bands propagate and widen, and small dilatant zones are observed as shear strain increases and concentrates. One of the two bands of the conjugate set widens up to 3 mm in width at an axial strain of 3.8%. From then, shear strain remains mainly localized in this band.

Inside the large band, density maps show a homogenization and a densification down to 30% of porosity, similar to the dense part of the sample. Inspection of reconstructed XRCT images reveals intensive grain crushing, with smaller dense grains embedded in fine-grained residuals provided by mostly shells and pulverized weak grains inside of the band and grain fracturing on both sides, with a limited range. The dense zone appears to remain essentially intact.

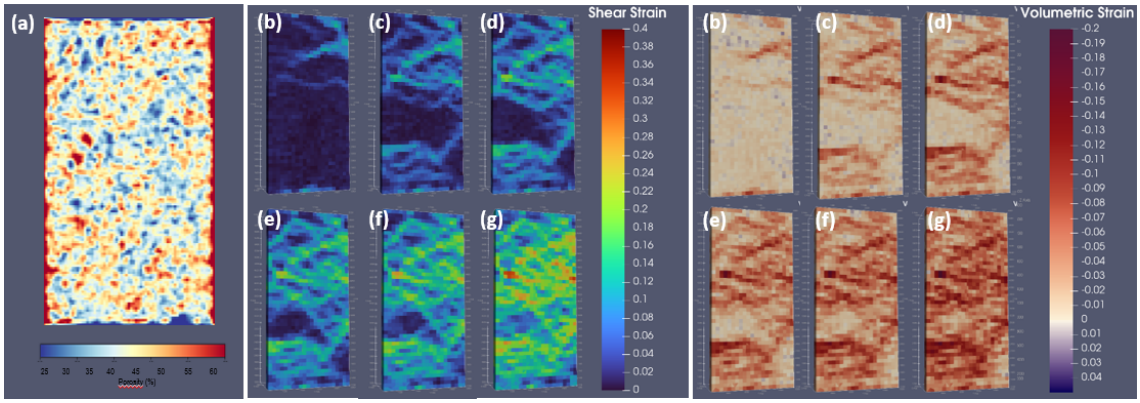


Figure 4. (a) Cross section through porosity map of the porous sample tested at a confining pressure of 6MPa before loading. In each point, the porosity is computed over a subvolume of 50 voxels (about 160 µm). Accumulated shear (center) and volumetric (right) strain in the sample tested at a confining pressure of 6MPa at various applied axial strain: (b) 0.77%, (c) 2.7%, (d) 4.2%, (e) 5.8%, (f) 7.4%, (g) 10.6%.

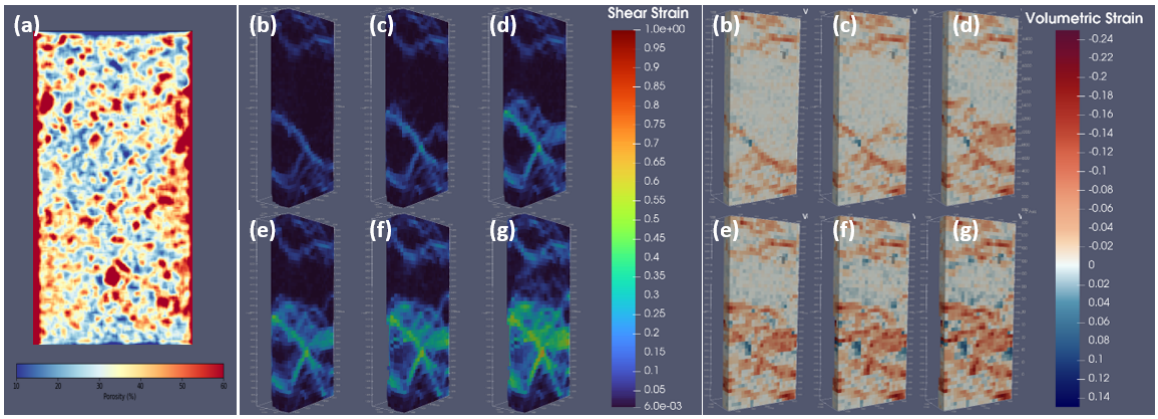


Figure 3. (a) Cross section through porosity map of the dense sample tested at a confining pressure of 6MPa before loading. In each point, the porosity is computed over a subvolume of 50 voxels (about 160 µm). Accumulated shear (center) and volumetric (right) strain inside the sample tested at a confining pressure of 6MPa at various applied axial strain: (b) 0.15%, (c) 2.1%, (d) 3.8%, (e) 5.8%, (f) 7.7%, (g) 9.8%.

## CONCLUSION

The formation of localized deformation bands in reservoir rocks may considerably affect the performance of geosystems. Given the complexity of the microstructure of carbonate rocks, *in situ* triaxial testing appears to be a very efficient way to investigate the involved micro-mechanisms of deformation, by imaging the sample during loading. Saint Maximin limestone exhibits porosity heterogeneity at the centimeter scale with an alternation of more porous and denser zones. Samples cored in these different zones show different mechanical responses and different localization patterns. In porous samples, which have a more homogeneous microstructure, compactant

deformation bands progressively saturate the sample leading to a quasi-homogeneous compaction. Strain is accommodated by the crushing of weaker grains. Dense samples, which have a more heterogeneous microstructure, exhibit highly localized thick deformation bands with zones of compaction and zones of dilatancy. They are characterized by intense crushing of the weaker grains, while strong smaller grains remain intact.

## ACKNOWLEDGEMENTS

This research has been carried out within the Energy4Climate Interdisciplinary Center (E4C) of Institut Polytechnique de Paris and Ecole des Ponts ParisTech and has benefited from the support of the 3rd Programme d'Investissements d'Avenir [ANR-18-EUR-0006-02]. The presented experiment at Synchrotron Soleil was run in the context of the standard proposal 20220588.

## REFERENCES

Abdallah Y. 2020. *Compaction banding in high-porosity limestones: Experimental observations and modelling*. PhD Manuscript, Université Paris-Est.

Abdallah Y., Sulem J., Bornert M., Ghabezloo S., Stefanou I. 2021. Compaction Banding in High-Porosity Carbonate Rocks: 1. Experimental Observations. *Journal of Geophysical Research: Solid Earth*, 126 (1), pp. 1–24.

Baud, P., Vinciguerra, S., David, C., Cavallo, A., Walker, E., & Reuschlé, T. 2009. Compaction and failure in high porosity carbonates: Mechanical data and microstructural observations. *Pure and Applied Geophysics, 166, pp. 869-898.*

Baud, P. Schubnel, A., Heap, M., Rolland, A. 2017. *Inelastic compaction in high-porosity limestone monitored using acoustic emissions.* Journal of Geophysical Research: Solid Earth, 122, 9989-10,008.

Huang, L., Baud, P., Cordonnier, B., Renard, F., Liu, L., & Fong Wong, T. 2019. *Synchrotron X-ray imaging in 4D: Multiscale failure and compaction localization in triaxially compressed porous limestone*. Earth and Planetary Science Letters, 528, 115831.

King, A., Guignot, N., Zerbino, P., Boulard, E., Desjardins, K., Bordessoule, M., Leclerq, N., Le, S., Renaud, G., Cerato, M., Bornert, M., Lenoir, N., Delzon, S., Perrillat, J.-P., Legodec, Y., Itié, J.-P. *Tomography and imaging at the PSICHE beam line of the SOLEIL synchrotron*, Review of Scientific Instruments, 87(9).

Lenoir, N., Bornert, M., Desrues, J. Bésuelle, P. and Viggiani, G. 2007. *Volumetric digital image correlation applied to X-Ray microtomography images form triaxial compression tests on argillaceous rocks*, Strain, 43, pp. 193-205.

Leuthold, J., Gerolymatou, E., & Triantafyllidis, T. 2021. *Effect of Compaction Banding on the Hydraulic Properties of Porous Rock - Part II: Constitutive Description and Numerical Simulations*. Rock Mechanics and Rock Engineering, 54 (6), 2685–2696.

Papazoglou, A., Shahin, G., Marinelli, F., Dano, C., Buscarnera, G., & Viggiani, G. 2017. *Localized Compaction in Tuffeau de Maastricht: Experiments and Modeling*. In (pp. 481–488).

Stanchits, S., Fortin, J., Gueguen, Y. and Dresen, G. 2009. *Initiation and Propagation of Compaction Bands in Dry and Wet Bentheim Sandstone*. Pure and Applied Geophysics.

Wong, T.-F. and Baud, P. 2012. *The brittle-ductile transition in porous rock: A review*. In: Journal of Structural Geology 44, pp. 25–53.